ACS APPLIED MATERIALS & INTERFACES

Research Article

Cite This: ACS Appl. Mater. Interfaces 2018, 10, 6982−6990

www.acsami.org

A Highly Sensitive Strategy for Fluorescence Imaging of MicroRNA in Living Cells and in Vivo Based on Graphene Oxide-Enhanced Signal Molecules Quenching of Molecular Beacon

Limin Yang, Bo Liu, Meimei Wang, Jia Li, Wei Pan, Xiaonan Gao, Na Li,* and Bo Tang*

College of Chemistry, Chemical Engineering and Materials Science, Collaborative Innovation Center of Functionalized Probes for Chemical Imaging in Universities of Shandong, Key Laboratory of Molecular and Nano Probes, Ministry of Education, Institute of Molecular and Nano Science, Shandong Normal University, Jinan 250014, P. R. China

Supporting Information

ABSTRACT: In situ imaging of microRNA (miRNA) in living cells and in vivo is beneficial for promoting the studies on miRNA-related physiological and pathological processes. However, the current strategies usually have a low signal-to-background ratio, which greatly affects the sensitivity and imaging performance. To solve this problem, we developed a highly sensitive strategy for fluorescence imaging of miRNA in living cells and in vivo based on graphene oxide (GO)-enhanced signal molecule quenching of a molecular beacon (MB). 2Cy5-MB was designed by coupling two Cy5 molecules onto the opposite ends of MB. The fluorescence intensities of two Cy5 molecules were reduced because of the self-quenching effect. After adsorbing on the GO surface, the fluorescence quenching of the molecules was enhanced by fluorescence resonance energy transfer. This double-quenching effect significantly reduced the fluorescence background. In the presence of one miRNA molecule, the fluorescence signals of two Cy5 molecules were simultaneously recovered. Therefore, a significantly enhanced signal-to-background ratio was obtained, which greatly improved the detection sensitivity. In the presence of miRNA, the fluorescence intensity of 2Cy5-MB-GO recovered about 156 times and the detection limit was 30 pM. Compared with 1Cy5-MB-GO, the elevated fluorescence intensity was enhanced 8 times and the detection limit was reduced by an order of magnitude. Furthermore, fluorescence imaging experiments demonstrated that 2Cy5-MB-GO could visually detect microRNA-21 in various cancer cells and tumor tissues. This simple and effective strategy provides a new sensing platform for highly sensitive detection and simultaneous imaging analysis of multiple low-level biomarkers in living cells and in vivo.

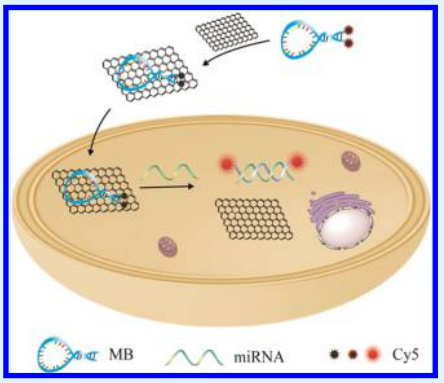

KEYWORDS: *double-quenching effect, enhanced signal-to-background ratio, high sensitivity, microRNA imaging, in vivo*

INTRODUCTION

MicroRNAs (miRNAs) play an important role in various biological processes. The abnormal expression of miRNAs is closely associated with many diseases.[1,2] It is noteworthy that the expression of intracellular miRNAs is low and even downregulated in some serious diseases.[3−5] Therefore, developing sensitive and effective methods for detecting miRNAs in living cells and in vivo is very important for biomedical research and clinical diagnosis of diseases. Traditional methods, such as real-time quantitative polymerase chain reaction (PCR), northern blotting, and microarray technology, are applicable for the detection of miRNAs only in homogeneous solutions and cell lysates.[6−11] In recent years, many fluorescence nanoprobes have been developed for detecting intracellular miRNAs.[12−17] However, the detection sensitivity of these methods was limited by the 1:1 reaction ratio, where a target molecule could restore the fluorescence of only one dye molecule. Therefore, several amplification methods for miRNA detection have been reported to improve the sensitivity. For example, rolling circle amplification-based strategies were developed for visually detecting miRNAs in a single cell.[18,19] However, they needed not only to fix the cells but also to deliver the enzymes into the cells, thus failing to real-time visualize miRNA in living cells and in vivo. Furthermore, assembled nanosensors and fuel DNA probes were also used for amplified detection of miRNAs in living cells.[20,21] However, the construction of these nanosensors and the additional transfection process are very tedious and time-consuming. In addition, the single-stranded sequences of fuel DNA probes are easily degraded by the enzymes after being delivered into the cells, which not only affects the sensitivity of intracellular miRNA detection but also makes it difficult to realize highly sensitive imaging of miRNA in vivo. As a result, a simple and sensitive method is still lacking for monitoring miRNAs in living cells and in vivo.

Received: December 19, 2017
Accepted: February 6, 2018
Published: February 6, 2018

DOI: 10.1021/acsami.7b19284
ACS Appl. Mater. Interfaces 2018, 10, 6982−6990

A molecular beacon (MB) can identify the specific nucleic acid target.[22−26] However, it is difficult for a MB to enter living cells. Even after transfection, it is very unstable in living cells owing to nuclease degradation. Although some nanoprobes were developed by modifying MBs onto the surface of gold nanoparticles via gold−sulfur bonds to improve the stability of nucleases,[27−30] the sensitivity was restricted because of the relatively high fluorescence background and the 1:1 reaction ratio. Moreover, the MB on the nanoprobe is released by the intracellular mercapto compounds, which decreases the stability of the nanoprobe and impacts the accuracy of detection. Graphene oxide (GO) is a good carrier and quencher.[31−33] The fluorescence nanoprobe based on GO is one of the most commonly used strategies for the detection of nucleic acid molecules.[34−37] GO could bind a single-dye-labeled ssDNA probe by the $\pi-\pi$ stacking effect between the ring structure of nucleobases and the hexagonal cells of GO.[38−40] The sp^2 aromatic domains within GO induced efficient fluorescence quenching of the dyes via fluorescence resonance energy transfer (FRET).[41−44] When a target molecule reacted with the DNA probe to form a duplex, it was released from the GO surface and restored the fluorescence of one dye molecule. This 1:1 relationship also restricts the detection sensitivity. It is thus a still-unresolved problem that can simultaneously reduce the fluorescence background and increase the detection signal to obtain the enhanced signal-to-noise ratio and further achieve highly sensitive detection and imaging of miRNAs in living cells and in vivo.

Herein, we separately labeled two Cy5 molecules onto the opposite ends of a single MB (2Cy5-MB). The distance between the two Cy5 molecules was close owing to the stem−loop structure of MB; therefore, the fluorescence signal of the 2Cy5-MB decreased by the self-quenching effect.[45] The fluorescence quenching of the 2Cy5-MB was further enhanced via FRET after the loop region of the MB was adsorbed on the surface of GO by $\pi-\pi$ stacking interaction. This double-quenching effect efficiently reduced the fluorescence background. In the presence of one target molecule, the 2Cy5-MB formed a duplex structure, which resulted in the release of 2Cy5-MB from GO and separated two Cy5 molecules. Therefore, the fluorescence signals of the two Cy5 molecules were restored, which implied that one target molecule was able to yield two signal outputs (1:2 reaction ratio). As a result, a significantly enhanced signal-to-background ratio was successfully obtained by coupling the effective reduced fluorescence background with the 1:2 reaction ratio. Taking microRNA-21 (miRNA-21) as the target model, about 156-fold increase in the fluorescence signal was achieved for 2Cy5-MB-GO in the presence of the miRNA-21 target and the detection limit was calculated to be 30 pM. The fluorescence imaging results demonstrated that 2Cy5-MB-GO was capable of highly sensitive imaging of miRNA-21 in living cells and tumor tissues. The details of this strategy are shown in Scheme 1.

Scheme 1. Illustration of the Formation of 2Cy5-MB-GO Complex and Its Application in miRNA Sensing

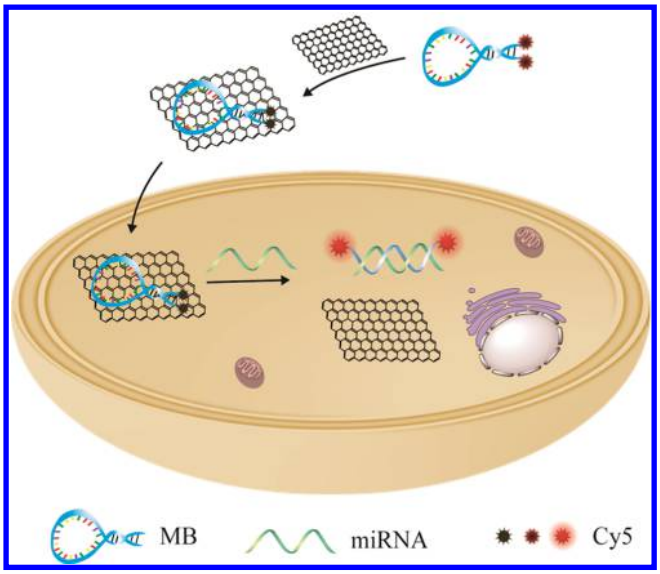

EXPERIMENTAL SECTION

Reagents and Materials. Sodium chloride (NaCl), potassium chloride (KCl), and magnesium chloride hexahydrate ($MgCl_2 \cdot 6H_2O$) were purchased from China National Pharmaceutical Group Corp. Graphene oxide (GO) was purchased from Nanjing XFNANO Materials Tech. Co., Ltd. (Nanjing, China). 3-(4,5-Dimethylthiazol-2-yl)-2,5-diphenyltetrazolium bromide (MTT) was acquired from Sigma-Aldrich. Deoxyribonuclease I (DNase I) was purchased from Solarbio Science and Technology Co., Ltd. (Beijing, China). Cell culture products, unless mentioned otherwise, were purchased from Hyclone. The human breast cancer cell line (MCF-7), human hepatocellular liver carcinoma cell line (HepG2), human cervical cancer cell line (HeLa), and heart myoblast cells H9C2 were purchased from Procell Life Science Co., Ltd. All of the DNA oligonucleotides were synthesized by Sangon Biotechnology Co. Ltd. (Shanghai, China) and are mentioned in Table S1.

Apparatus. High-resolution transmission electron microscopy (HRTEM) was carried out on a JEM-2100 electron microscope. Fluorescence spectra measurements were performed with an FLS-980 Edinburgh fluorescence spectrometer. The MTT assay was recorded using a microplate reader (Synergy 2, Biotek). Confocal fluorescence imaging experiments were carried out with a Leica TCS SP8 confocal laser scanning microscope with an objective lens (20×). Real-time (RT)-PCR was performed with a LineGene 9620 (Bioer, Binjiang, China). Flow cytometry was carried out on an ImageStreamX Mark II imaging flow cytometer (Merck Millipore). Fluorescence animal imaging was carried out on a Caliper IVIS Lumina III imaging system.

Fluorescence Quenching. For optimizing the concentration of GO, 2Cy5-MB (50 nM) was mixed with various concentrations of GO (0, 5, 8, 10, 15, 20, 30, 40, and 60 μg/mL) in Tris−HCl buffer solution (20 mM Tris, 100 mM NaCl, 5 mM KCl, and 1 mM $MgCl_2$). The above solutions were allowed to incubate for 10 min, and then the fluorescence intensities were recorded with $\lambda_{ex}/\lambda_{em}$ = 648/665 nm.

Kinetics Assay. To optimize the reaction time, the 2Cy5-MB (50 nM) was first mixed with GO solution in Tris−HCl buffer solution for 10 min. Then, the miRNA-21 target was added to the above solution. The fluorescence intensities were recorded with the increasing time (0, 2, 5, 10, 20, 30, 40, 50, and 60 min) with 648 nm excitation and 665 nm emission.

miRNA-21 Detection and Specificity Experiments. The detection of miRNA-21 was performed under optimal conditions. Various concentrations of miRNA-21 targets (0−800 nM) were added into 2Cy5-MB-GO in Tris−HCl buffer solution. After incubation for 30 min at 37 °C, the fluorescence intensities were excited at 648 nm and measured at 665 nm. Furthermore, the fluorescence intensities of 1Cy5-MB-GO were measured under different concentrations of miRNA-21 targets (0−800 nM). To investigate the selectivity for miRNA-21 detection, the complementary DNA targets (200 nM), mismatched targets (200 nM), and oxidative-stress-associated redox chemicals, including glutathione (10 mM) and hydrogen peroxide (H_2O_2, 100 μM), were studied using the same procedure as mentioned above.

Nuclease Assay. First, GO (10 μg/mL) was mixed with 50 nM 2Cy5-MB in Tris−HCl buffer solution for 10 min. Then, the experiments were divided into two groups. DNase I (2 U/L) was

DOI: 10.1021/acsami.7b19284
ACS Appl. Mater. Interfaces 2018, 10, 6982−6990

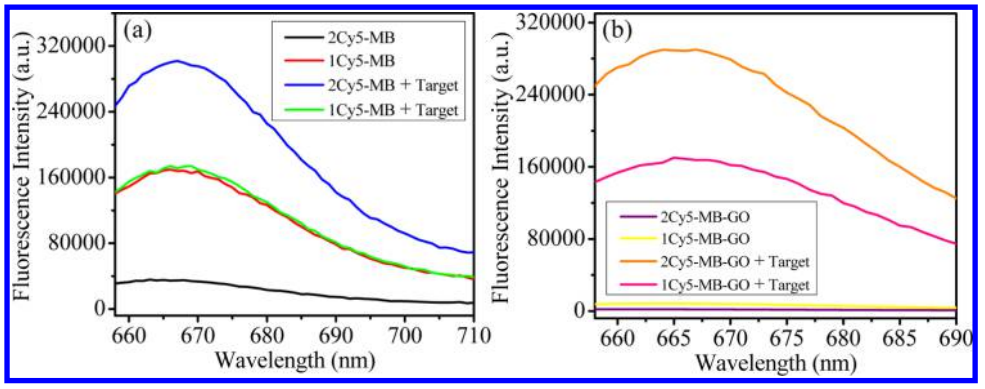

Figure 1. (a) Fluorescence spectra of 2Cy5-MB, 1Cy5-MB, 2Cy5-MB and Target, and 1Cy5-MB and Target. (b) Fluorescence spectra of 2Cy5-MB-GO, 1Cy5-MB-GO, 2Cy5-MB-GO and target, and 1Cy5-MB-GO and target. The concentration of the target was 800 nM. The excitation and emission wavelengths were 648 and 665 nm, respectively.

added to one group. Then, miRNA-21 targets (200 nM) were added to the above solution for 0.5 h. Another group without DNase I was set as the control. The fluorescence intensities were recorded with $\lambda_{ex}/\lambda_{em}$ = 648/665 nm.

Cytotoxicity Assay. The MTT assay was performed to study the cytotoxicity of GO. MCF-7 cells were dispersed within 96-well microtiter plates at 37 °C for 24 h. Then, various concentrations of GO (10, 20, and 40 μg/mL) were separately added into each well for 12 and 24 h. Then, the MTT solution (150 μL, 0.5 mg/mL in phosphate-buffered saline (PBS)) was further added to each well for another 4 h. After removing the remaining MTT medium, 150 μL of dimethyl sulfoxide was added to each well. The absorbance was measured at 490 nm with a microplate reader.

Cellular Uptake Mechanism of 2Cy5-GO-MB. MCF-7 cells were plated in glass-bottomed dishes for 24 h at 37 °C in a humidified atmosphere with 5% CO_2. MCF-7 cells were preincubated separately with different endocytosis inhibitors [20 μM chlorpromazine or 50 μM ethylisopropylamiloride (EIPA)] for 1.5 h. Then, 2Cy5-MB-GO was added and the dishes were incubated for 3 h. Each dish was washed three times with PBS buffer. Moreover, confocal fluorescence imaging studies were carried out with 633 nm excitation.

Confocal Fluorescence Imaging. MCF-7, HeLa, HepG2, and H9C2 cells were plated on chamber slides for 24 h. First, MCF-7 cells treated with 1 mL of 2Cy5-MB-GO in Dulbecco's modified Eagle's medium (DMEM) for different incubation times were studied. Then, MCF-7 and H9C2 cells were incubated separately with 2Cy5-MB-GO for 3 h. Finally, MCF-7, HeLa, and HepG2 cells were incubated separately with 2Cy5-MB-GO and 1Cy5-MB-GO solutions for 3 h. Before imaging, all of the cells were washed with PBS (pH 7.4) three times and visualized by confocal laser scanning microscopy. The images were obtained using excitation at 633 nm and an emission filter at 650−750 nm. The background parameters, including laser intensity, exposure time, and objective, were fixed in different fluorescence imaging tests.

RT-PCR. RT-PCR was carried out with SuperReal PreMix Plus (Tiangen) on LineGene 9620. MiRNA was isolated from the cells using the miRcute miRNA isolation kit (Tiangen). cDNA synthesis was carried out using the miRcute miRNA first-strand cDNA synthesis kit (Tiangen) in accordance with the manufacturer's instructions. The relative level of miRNA was calculated from the quantities of miRNA PCR and U6 PCR products.

Flow Cytometry. Before imaging, all three kinds of cells, MCF-7, HeLa, and HepG2, were cultured in cell dishes for 24 h. Then, 1 mL of 2Cy5-MB-GO and 1Cy5-MB-GO in DMEM was separately added to all of the cells at 37 °C. By the removal of the culture medium, all of the cells were digested with 1 mL of trypsin and washed three times with PBS. Finally, all of the cells were analyzed by a flow cytometer.

Establishment of Tumor Models and the in Vivo Imaging Assay. All animal experiments were carried out according to the Principles of Laboratory Animal Care (People's Republic of China). For the establishment of tumor models, breast tumor model establishment was used as an example to illustrate the procedure. MCF-7 cells (1×10^7) were injected subcutaneously into the right axillary region of the nude mice. The other tumor models (HeLa and HepG2 cells) were developed as mentioned above. For miRNA-21 imaging, 50 μL of 2Cy5-MB-GO and 1Cy5-MB-GO was injected separately into the tumor tissue for 1 h. Before imaging, the living mice were anesthetized using 4% chloral hydrate (200 μL). The mice were examined by the Caliper IVIS Lumina III imaging system with 620 nm excitation.

RESULTS AND DISCUSSION

Feasibility Study. We first studied whether the fluorescence intensities of the two Cy5 molecules were self-quenched when they were coupled at both the ends of the MB. One Cy5-molecule-labeled MB (1Cy5-MB) was synthesized for comparison. 2Cy5-MB and 1Cy5-MB had a stem−loop structure in buffer solution. As shown in Figure 1a, the fluorescence intensity of 2Cy5-MB (black curve) was much lower than that of 1Cy5-MB (red curve) when they were at the same concentration, clearly indicating that there was a self-quenching effect between two Cy5 molecules of 2Cy5-MB because of their small distance. Upon incubation with the targets, a significant fluorescence enhancement of 2Cy5-MB (blue curve) was observed, whereas the fluorescence signal of 1Cy5-MB (green curve) was almost unchanged. Notably, the fluorescence intensity of 2Cy5-MB was higher than that of 1Cy5-MB in the presence of targets, revealing that the fluorescence signals of the two Cy5 molecules were definitely recovered. All of these results demonstrated that the hairpin structure of 2Cy5-MB was opened and a duplex structure was formed in the presence of a target, which resulted in the separation of two Cy5 molecules and fluorescence recovery.

To verify the feasibility of the proposed strategy for miRNA detection, the proof-of-concept experiments were performed. The loop region of the MB can be strongly adsorbed on the surface of GO by the noncovalent $\pi-\pi$ stacking interaction. Therefore, 2Cy5-MB-GO can be simply prepared after mixing 2Cy5-MB with the GO solution. 1Cy5-MB-GO was also prepared for representing the traditional GO-based method for miRNA detection. The fluorescence intensities of 2Cy5-MB and 1Cy5-MB would be quenched after adsorption on the surface of GO. As shown in Figure 1b, the fluorescence intensity of 2Cy5-MB-GO (purple curve) was very low and was about 4.5-fold lower than that of 1Cy5-MB-GO (yellow curve). It clearly indicated that the double-quenching effect, including the self-quenching effect of two Cy5 molecules and the quenching effect of GO, significantly decreased the fluorescence

DOI: 10.1021/acsami.7b19284
ACS Appl. Mater. Interfaces 2018, 10, 6982−6990

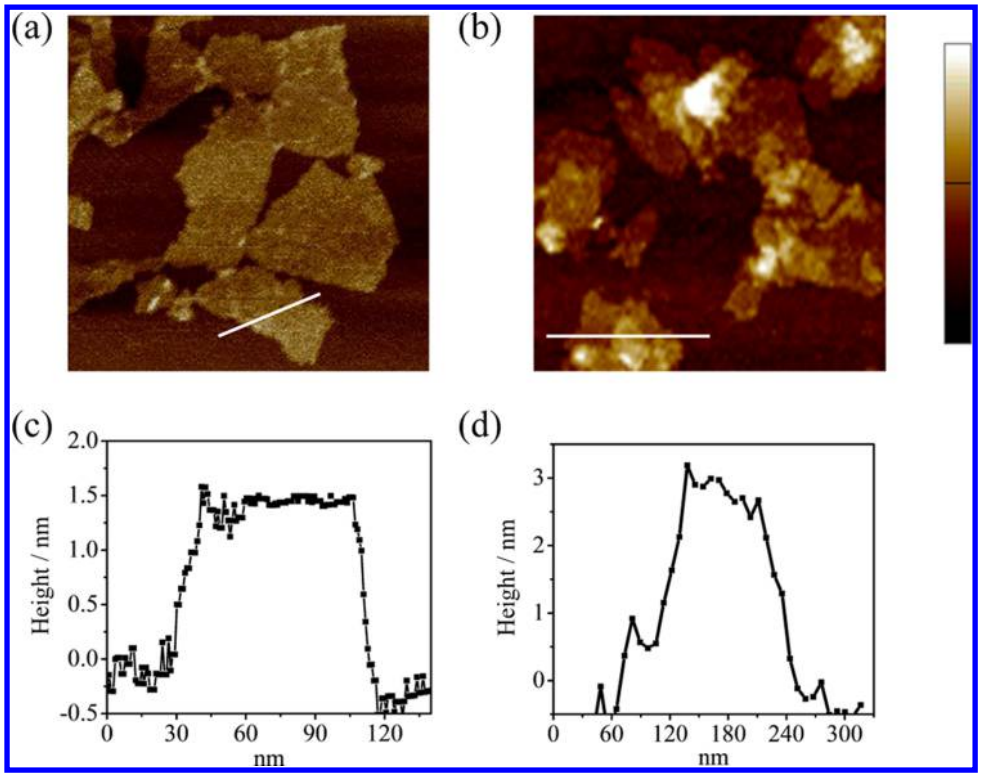

Figure 2. Atomic force microscopy images of GO (a) and 2Cy5-MB-GO (b). (c, d) Height profiles of the sections labeled with the white lines in images (a) and (b), respectively.

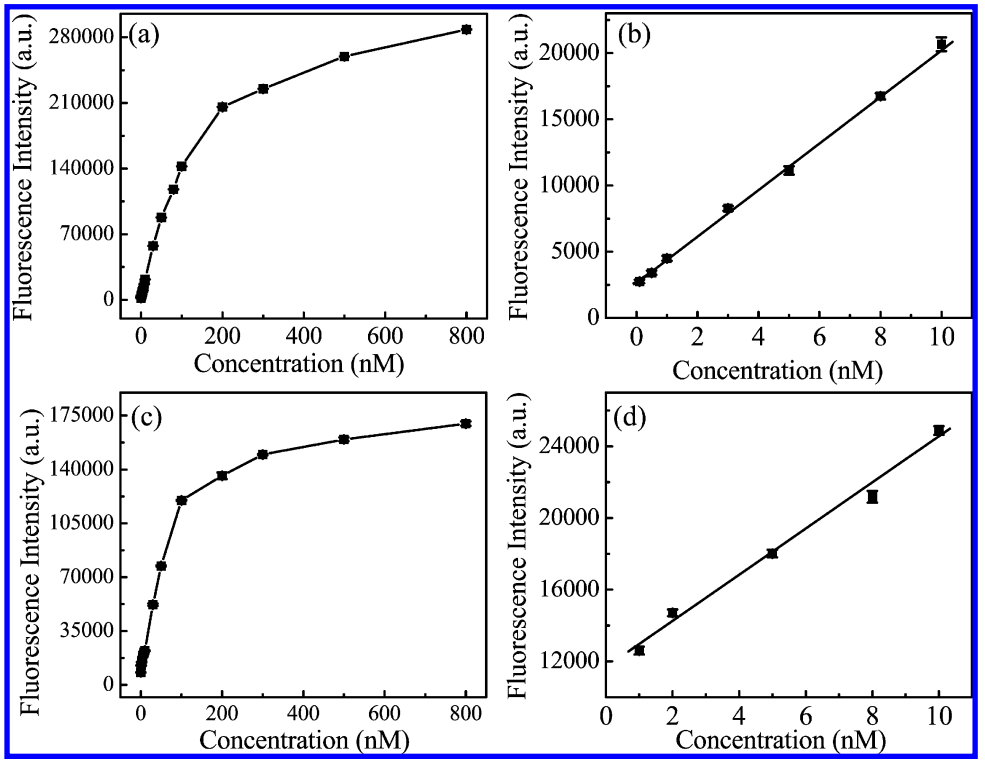

Figure 3. Fluorescence intensities of 2Cy5-MB-GO (a) and 1Cy5-MB-GO (c) in the presence of various concentrations of miRNA-21 targets (0−800 nM). Calibration curves corresponding to the fluorescence signals of 2Cy5-MB-GO (b) and 1Cy5-MB-GO (d) at different concentrations of miRNA-21 targets: (b) 0.1−10 nM and (d) 1−10 nM. The fluorescence intensities were recorded with $\lambda_{ex}/\lambda_{em}$ = 648/665 nm.

background. In the presence of targets, the fluorescence intensities of 2Cy5-MB-GO and 1Cy5-MB-GO were clearly increased and the enhanced fluorescence intensity of 2Cy5-MB-GO (orange curve) was clearly higher than that of 1Cy5-MB-GO (pink curve), which demonstrated that the fluorescence signals of two Cy5 molecules of 2Cy5-MB were restored. About 156-fold increase in the fluorescence signal was achieved for 2Cy5-MB-GO, whereas a nearly 19.6-fold increase in the

DOI: 10.1021/acsami.7b19284
ACS Appl. Mater. Interfaces 2018, 10, 6982−6990

fluorescence signal was achieved for 1Cy5-MB-GO after hybridization with the target. It is noteworthy to point out that the enhanced fluorescence signal of 2Cy5-MB-GO is about 8-fold higher than that of 1Cy5-MB-GO in the presence of targets, revealing that 2Cy5-MB-GO definitely exhibits much enhanced properties in higher signal-to-background ratio than 1Cy5-MB-GO.

Characterization. The properties of GO and 2Cy5-MB-GO were investigated. As shown in Figure S1, GO and 2Cy5-MB-GO had a sheet structure morphology and the size was about 50−500 nm. Furthermore, atomic force microscopy results indicated that the thickness of GO was about 1.5 nm (Figure 2a) and it increased to about 3 nm after the adsorption of 2Cy5-MB (Figure 2b). The results confirmed that 2Cy5-MB-GO was successfully prepared.

Optimization of the Experimental Conditions. To achieve the best sensing performance, the concentration of GO was optimized first. As shown in Figure S2, the fluorescence intensity of 2Cy5-MB decreased appreciably with the increasing concentration of GO. When the concentration of GO reached 10 μg/mL, the fluorescence of 2Cy5-MB was completely quenched. Therefore, 10 μg/mL GO was used in the following experiments. Furthermore, kinetic experiments showed that about 50-fold fluorescence enhancement was observed upon addition of target for 2 min, implying a fast reaction kinetics (Figure S3).

Sensitivity and Specificity. Then, the fluorescence responses of 2Cy5-MB-GO upon incubation with various concentrations of miRNA-21 targets were recorded. As shown in Figure 3a, the fluorescence intensities of 2Cy5-MB-GO dramatically enhanced with the increasing concentrations of miRNA-21 targets from 0 to 800 nM and a good linearity was obtained in the range of 0.1−10 nM (Figure 3b). Moreover, about 10-fold enhanced intensity was observed at 10 nM target. The regression equation was F = 1781.7 × [target] nM + 2621.28. The detection limit was calculated to be 30 pM (3σ/slope). In addition, the fluorescence intensity of 1Cy5-MB-GO increased with the increasing concentrations of miRNA-21 targets (Figure 3c) and a good linearity was obtained from 1 to 10 nM (Figure 3d). The regression equation was F = 1286.7 × [target] nM + 11 688.5. The detection limit was determined to be 440 pM. We could clearly find that the detection limit of 2Cy5-MB-GO was 1 order of magnitude lower than that of 1Cy5-MB-GO. Although the detection limit value was 1 order of magnitude higher than that based on assembled nanosensors and fuel DNA probes,[20] it was lower than that reported previously using the traditional GO-based method and was comparable to that of some amplification strategies as well.[35,46−48] These results confirmed that the proposed strategy with the reduced fluorescence background and 1:2 reaction relationship greatly improved the detection sensitivity. Subsequently, the specificity of 2Cy5-MB-GO was studied. As shown in Figure S4, 2Cy5-MB-GO displayed much higher fluorescence signal for miRNA-21 than other interferences, implying that 2Cy5-MB-GO was remarkably specific and sensitive to miRNA-21 and could be used to detect miRNA-21 in living cells without any interference.

Nuclease Stability. Before applying 2Cy5-MB-GO for detecting and visualizing miRNA-21 in living cells, DNase I was used to evaluate the stability of 2Cy5-MB-GO under physiological conditions. As shown in Figure S5, a negligible change in fluorescence intensity was observed when 2Cy5-MB-GO was treated with DNase I. However, the fluorescence intensity increased greatly after adding the miRNA-21 target. This verified that 2Cy5-MB-GO exhibited high resistance to nuclease, which could be attributed to a steric hindrance effect of GO that prevents DNase I from contacting 2Cy5-MB.[49]

MTT Assay and Cellular Uptake Mechanism. To investigate the cytotoxicity of GO, an MTT assay was performed. The cells were incubated separately with 10, 20, and 40 μg/mL of GO for 12 and 24 h. As shown in Figure S6, the cell viability was more than 95% under these conditions, suggesting that GO exhibited almost no cytotoxicity or side effects in living cells. This demonstrated that GO was a biofriendly carrier for efficient intracellular delivery.

To study whether GO can be used as a carrier for transporting MB into living cells, the fluorescence imaging was performed after HeLa cells were separately incubated with 2Cy5-MB, 1Cy5-MB, 2Cy5-MB-GO, and 1Cy5-MB-GO. As can be seen from Figure S7, the fluorescence signal of HeLa cells incubated with 2Cy5-MB-GO was higher than that of HeLa cells incubated with 2Cy5-MB. Similarly, the fluorescence signal of HeLa cells incubated with 1Cy5-MB-GO was higher than that of HeLa cells treated with 1Cy5-MB (Figure S8). These results indicated that GO was an efficient carrier for transporting MB into living cells.

Then, the internalization pathways of 2Cy5-MB-GO into living cells were investigated by applying various endocytosis inhibitors. Chlorpromazine was used to inhibit clathrin-mediated endocytosis. EIPA was used to inhibit macropinocytosis. Decreased fluorescence signals were observed after treatment with these inhibitors, suggesting that clathrin-mediated and macropinocytosis pathways made the contribution to the cellular uptake of 2Cy5-MB-GO (Figure 4).

Imaging of MiRNA in Living Cells. After investigating the characteristics of 2Cy5-MB-GO, we proceeded to explore its ability toward imaging miRNA-21 in living cells. We first studied the response of 2Cy5-MB-GO in MCF-7 cells with different incubation times. As shown in Figure S9, MCF-7 cells did not show detectable fluorescence without 2Cy5-MB-GO. After incubating with 2Cy5-MB-GO, MCF-7 cells showed gradually increasing fluorescence intensities with the increase in incubation time. The fluorescence signals reached the maximum at 3 h and then did not increase further. This suggested that the incubation time of 3 h should be appropriate in the following experiments.

Previous studies reported that the levels of miRNA-21 in cancer cells were higher than those in normal cells. Therefore, we intended to examine whether 2Cy5-MB-GO could detect the difference of miRNA-21 levels between tumor cell and normal cell. The cancer cell line (MCF-7) and the normal cell line (H9C2) were chosen as the positive and the negative cell, respectively. As shown in Figure S10a, the red fluorescence signal was strong after MCF-7 cells were incubated with 2Cy5-MB-GO, whereas a faint red fluorescence signal was observed when H9C2 cells were incubated with 2Cy5-MB-GO under the same conditions (Figure S10b). Furthermore, RT-PCR results were in good agreement with the confocal fluorescence imaging experiments (Figure S10e), further indicating that the fluorescence signals of 2Cy5-MB-GO correlated very well with the expression levels of miRNA-21. All of these results indicated that 2Cy5-MB-GO is able to detect the difference of miRNA-21 levels between tumor cell and normal cell.

To further explore the sensitivity and universality of the proposed method, three types of tumor cells, MCF-7, HepG2 and HeLa, were chosen in the following experiments. As shown

DOI: 10.1021/acsami.7b19284
ACS Appl. Mater. Interfaces 2018, 10, 6982−6990

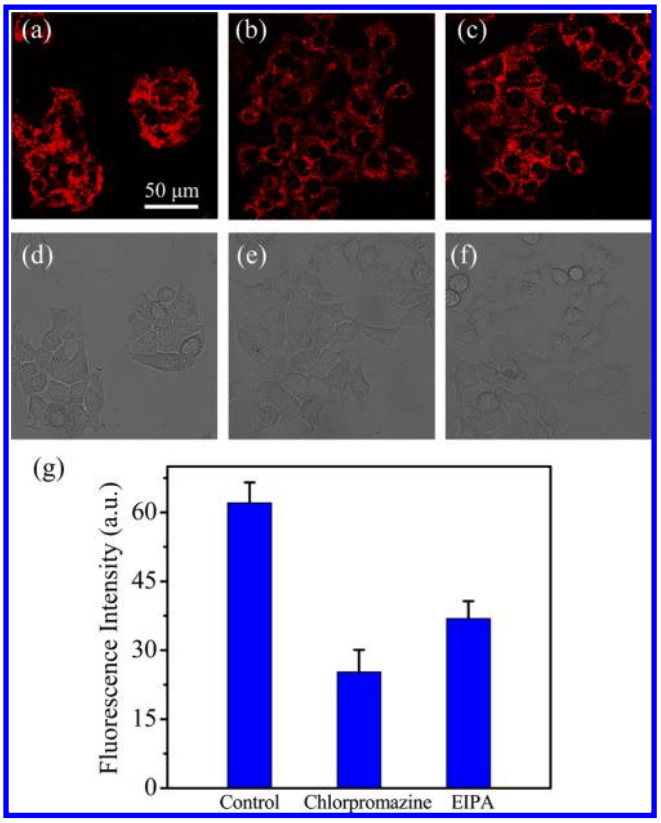

Figure 4. Cellular uptake pathways. The treated and untreated MCF-7 cells were incubated with 2Cy5-GO-MB. (a, d) Control groups, (b, e) chlorpromazine-treated groups, and (c, f) EIPA-treated groups. (d), (e), and (f) bright-field images of (a), (b), and (c), respectively. Scale bars are 50 μm. (g) Normalized fluorescence intensities of (a)−(c).

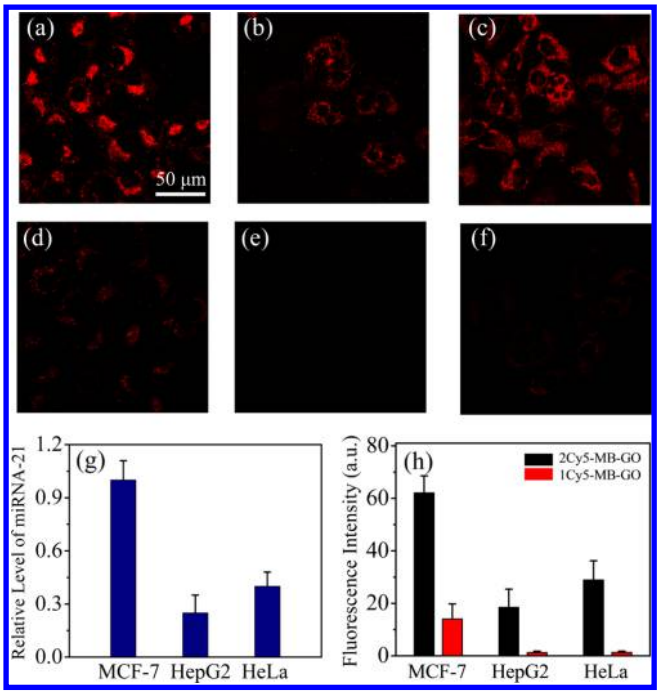

Figure 5. Confocal fluorescence images of MCF-7 (a, d), HepG2 (b, e), and HeLa (c, f) cells incubated separately with 2Cy5-GO-MB (a−c) and 1Cy5-GO-MB (d−f). The excitation wavelength is 633 nm. Scale bars are 50 μm. (g) Relative expression levels of miRNA-21 in MCF-7, HepG2, and HeLa cells. (h) Average fluorescence intensities of MCF-7, HepG2, and HeLa cells incubated separately with 2Cy5-MB-GO and 1Cy5-MB-GO.

in Figure 5a−c, different fluorescence intensities were observed when these cells were incubated with 2Cy5-MB-GO under the same conditions. MCF-7 cells displayed the highest fluorescence intensity, whereas HepG2 cells showed the lowest fluorescence intensity. This suggested that the relative levels of miRNA-21 in HeLa cells were lower than those in MCF-7 cells and higher than those in HepG2 cells. Furthermore, RT-PCR results were consistent with those of confocal fluorescence imaging experiments (Figure 5g). These results indicated that 2Cy5-MB-GO had sufficient sensitivity to visualize and detect miRNA-21 in these cancer cells. Then, the three kinds of cells incubated with 1Cy5-MB-GO were further observed. As shown in Figure 5d−f, the fluorescence signal of MCF-7 cells was higher than that of HepG2 and HeLa cells when these cells were incubated with 1Cy5-MB-GO, whereas similar and weak fluorescence signals were observed after the HepG2 and HeLa cells were treated with 1Cy5-MB-GO, indicating that 1Cy5-MB-GO could not visualize the different expression levels of miRNA-21 in these cells. Moreover, we can find that the same kind of cells incubated with 2Cy5-MB-GO displayed much higher fluorescence intensities than those of the cells treated with 1Cy5-MB-GO (Figure 5h). Moreover, flow cytometry experiments were performed to quantify the intracellular fluorescence signaling of these cells. The treated cells were harvested and washed, and then the cell-associated fluorescence was determined by flow cytometry. The results of flow cytometric analysis were consistent with the results of fluorescence imaging experiments (Figures 6 and S11). All of these results clearly demonstrated that 2Cy5-MB-GO showed a more superior performance than that of 1Cy5-MB-GO for in situ imaging of miRNA-21 levels in different living cells, which can be attributed to the increased sensitivity of 2Cy5-MB-GO.

Imaging of MiRNA in Vivo. To further assess the practicability of 2Cy5-MB-GO to image miRNA-21 in vivo, three xenograft tumor models (mice treated separately with MCF-7, HeLa, and HepG2 cells) were used. As shown in Figure 7a−c, different fluorescence intensities were observed after the tumor tissues were injected with 2Cy5-MB-GO, validating that 2Cy5-MB-GO was capable of visualizing and differentiating the miRNA-21 native variance in different tumor tissues. These results were consistent with the confocal fluorescence imaging results in living cells. However, after being injected with 1Cy5-MB-GO, although the fluorescence signals of MCF-7-cell-implanted tumors were higher than those of HepG2- and HeLa-cell-implanted tumors, the fluorescence intensities were similar in HepG2- and HeLa-cell-implanted tumors (Figure 7d−f). This suggested that 1Cy5-MB-GO could not image the different expression levels of miRNA-21 in these implanted tumors. Moreover, we can find that 2Cy5-MB-GO-treated tumor tissues display much higher fluorescence signals than those of 1Cy5-MB-GO-treated tumor tissues in the same kind of cell-implanted tumors (Figure 7g), implying that 2Cy5-MB-GO was more suitable than 1Cy5-MB-GO in practical applications with a great accuracy and reliability for miRNA-21 detection in vivo.

CONCLUSIONS

In summary, to improve the signal-to-background ratio of the current methods for miRNA detection in living cells and in vivo, a simple strategy was proposed for highly sensitive fluorescence imaging of miRNA in living cells and in vivo based

DOI: 10.1021/acsami.7b19284
ACS Appl. Mater. Interfaces 2018, 10, 6982−6990

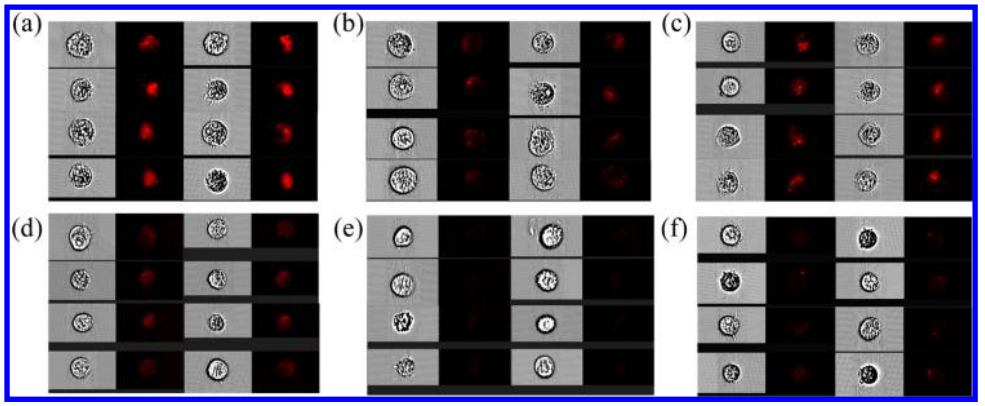

Figure 6. Flow cytometry. Images of MCF-7 (a, d), HepG2 (b, e), and HeLa (c, f) cells incubated separately with 2Cy5-MB-GO (a–c) and 1Cy5-MB-GO (d–f).

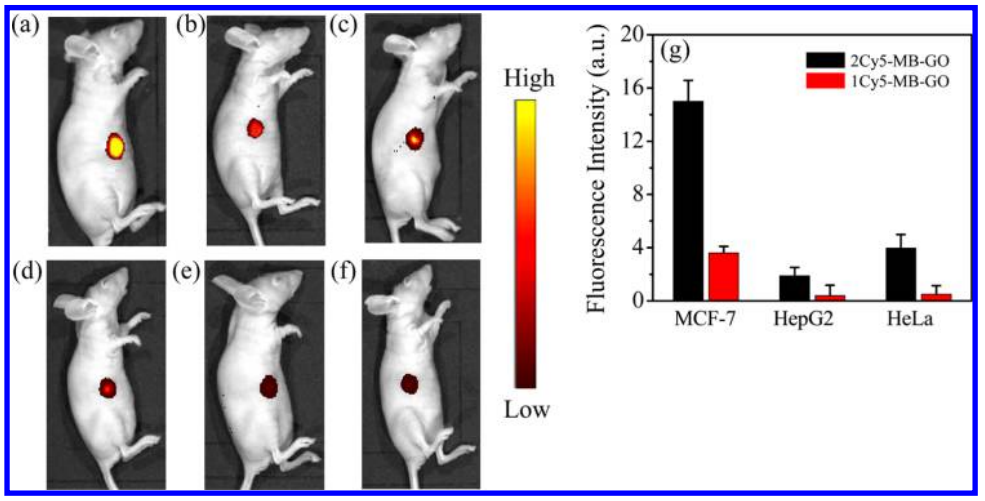

Figure 7. In vivo imaging of three different xenograft tumor models: MCF-7 (a, d), HepG2 (b, e), and HeLa (c, f). The mice were imaged with an excitation wavelength at 620 nm. (a–c) Tumor tissues were injected with 2Cy5-MB-GO. (d–f) Tumor tissues were injected with 1Cy5-MB-GO. (g) Quantification of the fluorescence intensities of three tumor models. Black and red bars stand for 2Cy5-MB-GO and 1Cy5-MB-GO, respectively.

on GO-enhanced signal molecules quenching of MB. A significantly enhanced signal-to-background ratio was successfully obtained through the reduced background and the 1:2 recovery ratio. The experimental results showed that about 156-fold increase of the fluorescence signal was achieved for 2Cy5-MB-GO in the presence of the miRNA target, and the detection limit was calculated to be 30 pM. Moreover, the fluorescence imaging results demonstrated that 2Cy5-MB-GO with a high sensitivity was able to detect miRNA-21 in different living cells and tumor tissues. We expect that this universal strategy will provide a new sensing platform for highly sensitive imaging of a variety of disease-related nucleic acid molecules in living cells and in vivo.

■ ASSOCIATED CONTENT

Supporting Information

The Supporting Information is available free of charge on the ACS Publications website at DOI: 10.1021/acsami.7b19284.

HRTEM images, fluorescence quenching, kinetics assay, specificity, MTT, confocal fluorescence imaging, and flow cytometry experiments (PDF)

■ AUTHOR INFORMATION

Corresponding Authors

*E-mail: lina@sdnu.edu.cn (N.L.).
*E-mail: tangb@sdnu.edu.cn (B.T.).

ORCID

Bo Tang: 0000-0002-8712-7025

Notes

The authors declare no competing financial interest.

■ ACKNOWLEDGMENTS

This work was supported by National Natural Science Foundation of China (21390411, 21535004, 91753111, and 21775094), Natural Science Foundation of Shandong Province (JQ201503 and ZR2015BQ003), and Science and Technology Planning Project of Higher Education of Shandong Province (J15LC06).

■ REFERENCES

(1) Arner, P.; Kulyté, A. MicroRNA Regulatory Networks in Human Adipose Tissue and Obesity. *Nat. Rev. Endocrinol.* **2015**, *11*, 276–288.
(2) van Rooij, E.; Olson, E. N. MicroRNA Therapeutics for Cardiovascular Disease: Opportunities and Obstacles. *Nat. Rev. Drug Discovery* **2012**, *11*, 860–872.
(3) Jazbutyte, V.; Thum, T. MicroRNA-21: from Cancer to Cardiovascular Disease. *Curr. Drug Targets* **2010**, *11*, 926–935.

DOI: 10.1021/acsami.7b19284
ACS Appl. Mater. Interfaces 2018, 10, 6982–6990

(4) Ryan, B. M.; Robles, A. I.; Harris, C. C. Genetic Variation in MicroRNA Networks: the Implications for Cancer Research. *Nat. Rev. Cancer* **2010**, *10*, 389−402.
(5) Wu, L.; Qu, X. Cancer Biomarker Detection: Recent Achievements and Challenges. *Chem. Soc. Rev.* **2015**, *44*, 2963−2997.
(6) Castoldi, M.; Schmidt, S.; Benes, V.; Noerholm, M.; Kulozik, A. E.; Hentze, M. W.; Muckenthaler, M. U. A Sensitive Array for MicroRNA Expression Profiling (miChip) Based on Locked Nucleic Acids (LNA). *RNA* **2006**, *12*, 913−920.
(7) Deng, R.; Zhang, K.; Li, J. Isothermal Amplification for MicroRNA Detection: From the Test Tube to the Cell. *Acc. Chem. Res.* **2017**, *50*, 1059−1068.
(8) Dong, H.; Lei, J.; Ding, L.; Wen, Y.; Ju, H.; Zhang, X. MicroRNA: Function, Detection, and Bioanalysis. *Chem. Rev.* **2013**, *113*, 6207−6233.
(9) Sun, Y.; Tian, H.; Liu, C.; Sun, Y.; Li, Z. One-step Detection of MicroRNA with High Sensitivity and Specificity via Target-Triggered Loop-Mediated Isothermal Amplification (TT-LAMP). *Chem. Commun.* **2017**, *53*, 11040−11043.
(10) Ryoo, S.-R.; Lee, J.; Yeo, J.; Na, H.-K.; Kim, Y.-K.; Jang, H.; Lee, J. H.; Han, S. W.; Lee, Y.; Kim, V. N.; Min, D.-H. Quantitative and Multiplexed MicroRNA Sensing in Living Cells Based on Peptide Nucleic Acid and Nano Graphene Oxide (PANGO). *ACS Nano* **2013**, *7*, 5882−5891.
(11) Várallyay, É.; Burgyán, J.; Havelda, Z. MicroRNA Detection by Northern Blotting using Locked Nucleic Acid Probes. *Nat. Protoc.* **2008**, *3*, 190−196.
(12) Choi, C. K. K.; Li, J.; Wei, K.; Xu, Y. J.; Ho, L. W. C.; Zhu, M.; To, K. K. W.; Choi, C. H. J.; Bian, L. A Gold@Polydopamine Core−Shell Nanoprobe for Long-Term Intracellular Detection of MicroRNAs in Differentiating Stem Cells. *J. Am. Chem. Soc.* **2015**, *137*, 7337−7346.
(13) Dong, H.; Lei, J.; Ju, H.; Zhi, F.; Wang, H.; Guo, W.; Zhu, Z.; Yan, F. Target-Cell-Specific Delivery, Imaging, and Detection of Intracellular MicroRNA with a Multifunctional SnO_2 Nanoprobe. *Angew. Chem., Int. Ed.* **2012**, *51*, 4607−4612.
(14) Li, S.; Xu, L.; Sun, M.; Wu, X.; Liu, L.; Kuang, H.; Xu, C. Hybrid Nanoparticle Pyramids for Intracellular Dual MicroRNAs Biosensing and Bioimaging. *Adv. Mater.* **2017**, *29*, No. 1606086.
(15) Li, S.; Xu, L.; Ma, W.; Wu, X.; Sun, M.; Kuang, H.; Wang, L.; Kotov, N. A.; Xu, C. Dual-Mode Ultrasensitive Quantification of MicroRNA in Living Cells by Chiroplasmonic Nanopyramids Self-Assembled from Gold and Upconversion Nanoparticles. *J. Am. Chem. Soc.* **2016**, *138*, 306−312.
(16) Luan, M.; Li, N.; Pan, W.; Yang, L.; Yu, Z.; Tang, B. Simultaneous Detection of Multiple Targets Involved in the PI3K/AKT Pathway for Investigating Cellular Migration and Invasion with a Multicolor Fluorescent Nanoprobe. *Chem. Commun.* **2017**, *53*, 356−359.
(17) Yang, L.; Ren, Y.; Pan, W.; Yu, Z.; Tong, L.; Li, N.; Tang, B. Fluorescent Nanocomposite for Visualizing Cross-Talk between MicroRNA-21 and Hydrogen Peroxide in Ischemia−Reperfusion Injury in Live Cells and In Vivo. *Anal. Chem.* **2016**, *88*, 11886−11891.
(18) Deng, R.; Tang, L.; Tian, Q.; Wang, Y.; Lin, L.; Li, J. Toehold-Initiated Rolling Circle Amplification for Visualizing Individual MicroRNAs In Situ in Single Cells. *Angew. Chem., Int. Ed.* **2014**, *53*, 2389−2393.
(19) Zhang, Z.; Wang, Y.; Zhang, N.; Zhang, S. Self-Assembly of Nucleic Acid Molecular Aggregates Catalyzed by a Triple-Helix Probe for miRNA Detection and Single Cell Imaging. *Chem. Sci.* **2016**, *7*, 4184−4189.
(20) He, X.; Zeng, T.; Li, Z.; Wang, G.; Ma, N. Catalytic Molecular Imaging of MicroRNA in Living Cells by DNA-Programmed Nanoparticle Disassembly. *Angew. Chem., Int. Ed.* **2016**, *55*, 3073−3076.
(21) Li, D.; Zhou, W.; Yuan, R.; Xiang, Y. A DNA-Fueled and Catalytic Molecule Machine Lights Up Trace Under-Expressed MicroRNAs in Living Cells. *Anal. Chem.* **2017**, *89*, 9934−9940.
(22) Kang, W. J.; Cho, Y. L.; Chae, J. R.; Lee, J. D.; Choi, K.-J.; Kim, S. Molecular Beacon-Based Bioimaging of Multiple MicroRNAs during Myogenesis. *Biomaterials* **2011**, *32*, 1915−1922.
(23) Kuang, T.; Chang, L.; Peng, X.; Hu, X.; Gallego-Perez, D. Molecular Beacon Nano-Sensors for Probing Living Cancer Cells. *Trends Biotechnol.* **2017**, *35*, 347−359.
(24) Tyagi, S.; Kramer, F. R. Molecular Beacons: Probes That Fluoresce upon Hybridization. *Nat. Biotechnol.* **1996**, *14*, 303−308.
(25) Wang, Y.; Li, J.; Jin, J.; Wang, H.; Tang, H.; Yang, R.; Wang, K. Strategy for Molecular Beacon Binding Readout: Separating Molecular Recognition Element and Signal Reporter. *Anal. Chem.* **2009**, *81*, 9703−9709.
(26) Zheng, J.; Yang, R.; Shi, M.; Wu, C.; Fang, X.; Li, Y.; Li, J.; Tan, W. Rationally Designed Molecular Beacons for Bioanalytical and Biomedical Applications. *Chem. Soc. Rev.* **2015**, *44*, 3036−3055.
(27) Jayagopal, A.; Halfpenny, K. C.; Perez, J. W.; Wright, D. W. Hairpin DNA-Functionalized Gold Colloids for the Imaging of mRNA in Live Cells. *J. Am. Chem. Soc.* **2010**, *132*, 9789−9796.
(28) Li, N.; Chang, C.; Pan, W.; Tang, B. A Multicolor Nanoprobe for Detection and Imaging of Tumor-Related mRNAs in Living Cells. *Angew. Chem., Int. Ed.* **2012**, *51*, 7426−7430.
(29) Pan, W.; Zhang, T.; Yang, H.; Diao, W.; Li, N.; Tang, B. Multiplexed Detection and Imaging of Intracellular mRNAs using a Four-Color Nanoprobe. *Anal. Chem.* **2013**, *85*, 10581−10588.
(30) Yang, L.; Chen, Y.; Pan, W.; Wang, H.; Li, N.; Tang, B. Visualizing the Conversion Process of Alcohol-Induced Fatty Liver to Steatohepatitis In Vivo with a Fluorescent Nanoprobe. *Anal. Chem.* **2017**, *89*, 6196−6201.
(31) Kundu, A.; Nandi, S.; Layek, R. K.; Nandi, A. K. Fluorescence Resonance Energy Transfer from Sulfonated Graphene to Riboflavin: A Simple Way to Detect Vitamin B2. *ACS Appl. Mater. Interfaces* **2013**, *5*, 7392−7399.
(32) He, Y.; Huang, G.; Cui, H. Quenching the Chemiluminescence of Acridinium Ester by Graphene Oxide for Label-Free and Homogeneous DNA Detection. *ACS Appl. Mater. Interfaces* **2013**, *5*, 11336−11340.
(33) Reina, G.; González-Domínguez, J. M.; Criado, A.; Vázquez, E.; Bianco, A.; Prato, M. Promises, Facts and Challenges for Graphene in Biomedical Applications. *Chem. Soc. Rev.* **2017**, *46*, 4400−4416.
(34) Liu, X.; Aizen, R.; Freeman, R.; Yehezkeli, O.; Willner, I. Multiplexed Aptasensors and Amplified DNA Sensors Using Functionalized Graphene Oxide: Application for Logic Gate Operations. *ACS Nano* **2012**, *6*, 3553−3563.
(35) Lu, C.-H.; Yang, H.-H.; Zhu, C.-L.; Chen, X.; Chen, G.-N. A Graphene Platform for Sensing Biomolecules. *Angew. Chem., Int. Ed.* **2009**, *48*, 4785−4787.
(36) He, S.; Song, B.; Li, D.; Zhu, C.; Qi, W.; Wen, Y.; Wang, L.; Song, S.; Fang, H.; Fan, C. A Graphene Nanoprobe for Rapid, Sensitive, and Multicolor Fluorescent DNA Analysis. *Adv. Funct. Mater.* **2010**, *20*, 453−459.
(37) Liu, B.; Salgado, S.; Maheshwari, V.; Liu, J. DNA Adsorbed on Graphene and Graphene Oxide: Fundamental Interactions, Desorption and Applications. *Curr. Opin. Colloid Interface Sci.* **2016**, *26*, 41−49.
(38) Li, W.; Hou, T.; Wu, M.; Li, F. Label-Free Fluorescence Strategy for Sensitive MicroRNA Detection Based on Isothermal Exponential Amplification and Graphene Oxide. *Talanta* **2016**, *148*, 116−121.
(39) Li, L.; Feng, J.; Liu, H.; Li, Q.; Tong, L.; Tang, B. Two-Color Imaging of MicroRNA with Enzyme-Free Signal Amplification via Hybridization Chain Reactions in Living Cells. *Chem. Sci.* **2016**, *7*, 1940−1945.
(40) Lu, C.; Huang, Z.; Liu, B.; Liu, Y.; Ying, Y.; Liu, J. Poly-cytosine DNA as a High-Affinity Ligand for Inorganic Nanomaterials. *Angew. Chem., Int. Ed.* **2017**, *56*, 6208−6212.
(41) Loh, K. P.; Bao, Q.; Eda, G.; Chhowalla, M. Graphene Oxide as a Chemically Tunable Platform for Optical Applications. *Nat. Chem.* **2010**, *2*, 1015−1024.
(42) Wang, L.; Pu, K.-Y.; Li, J.; Qi, X.; Li, H.; Zhang, H.; Fan, C.; Liu, B. A Graphene-Conjugated Oligomer Hybrid Probe for Light-Up

DOI: 10.1021/acsami.7b19284
ACS Appl. Mater. Interfaces 2018, 10, 6982−6990

Sensing of Lectin and *Escherichia Coli*. *Adv. Mater.* **2011**, *23*, 4386–4391.
(43) Liu, B.; Sun, Z.; Zhang, X.; Liu, J. Mechanisms of DNA Sensing on Graphene Oxide. *Anal. Chem.* **2013**, *85*, 7987–7993.
(44) Liu, Z.; Chen, S.; Liu, B.; Wu, J.; Zhou, Y.; He, L.; Ding, J.; Liu, J. Intracellular Detection of ATP Using an Aptamer Beacon Covalently Linked to Graphene Oxide Resisting Nonspecific Probe Displacement. *Anal. Chem.* **2014**, *86*, 12229–12235.
(45) Nesterova, I. V.; Erdem, S. S.; Pakhomov, S.; Hammer, R. P.; Soper, S. A. Phthalocyanine Dimerization-Based Molecular Beacons Using Near-IR Fluorescence. *J. Am. Chem. Soc.* **2009**, *131*, 2432–2433.
(46) Lu, Z.; Zhang, L.; Deng, Y.; Li, S.; He, N. Graphene Oxide for Rapid MicroRNA Detection. *Nanoscale* **2012**, *4*, 5840–5842.
(47) Cui, L.; Lin, X.; Lin, N.; Song, Y.; Zhu, Z.; Chen, X.; Yang, C. J. Graphene Oxide-Protected DNA Probes for Multiplex MicroRNA Analysis in Complex Biological Samples Based on a Cyclic Enzymatic Amplification Method. *Chem. Commun.* **2012**, *48*, 194–196.
(48) Wu, Y.; Huang, J.; Yang, X.; Yang, Y.; Quan, K.; Xie, N.; Li, J.; Ma, C.; Wang, K. Gold Nanoparticle Loaded Split-DNAzyme Probe for Amplified miRNA Detection in Living Cells. *Anal. Chem.* **2017**, *89*, 8377–8383.
(49) Wang, Y.; Li, Z.; Hu, D.; Lin, C.-T.; Li, J.; Lin, Y. Aptamer/Graphene Oxide Nanocomplex for in Situ Molecular Probing in Living Cells. *J. Am. Chem. Soc.* **2010**, *132*, 9274–9276.

DOI: 10.1021/acsami.7b19284
ACS Appl. Mater. Interfaces 2018, 10, 6982–6990